Effect of bending on single-walled carbon nanotubes: A Raman scattering study

Bei Wang,[1] Awnish K. Gupta,[1] Jun Huang,[2] Harindra Vedala,[2] Qingzhen Hao,[1] Vincent H. Crespi,[1,3,*] Wonbong Choi,[2] and Peter C. Eklund[1,3]

[1]*Department of Physics, Penn State University, University Park, Pennsylvania 16802, USA*

[2]*Department of Mechanical and Materials Engineering, Florida International University, Miami, Florida 33174, USA*

[3]*Department of Materials Science & Engineering, Materials Research Institute, Penn State University, University Park, Pennsylvania 16802, USA*

(Received 30 August 2009; revised manuscript received 1 February 2010; published 12 March 2010)

We describe microRaman studies of serpentine single-walled carbon nanotubes grown on single-crystal quartz. Local Raman spectra were collected from bent and straight segments of the same nanotube to elucidate the effects of bending. Bending radii as large as 1–2 μm produce a measurable shift of the frequencies of the G, D, and 2D bands while the radial breathing mode remains nearly unaffected by bending. The frequency shift is approximately linear in the bending curvature $1/R_b$ for radii of curvature R_b between 0.6 and 3.0 μm. A very tightly bent bundle with $R_b \sim 50$ nm develops a very intricate G-band structure caused by new Raman modes that are activated by the broken cylindrical symmetry. These results show diverse behavior depending on the nanotube wrapping indices (n,m) but are comparable in magnitude to those predicted by tight-binding calculations of the Raman response in bent tubes.

DOI: 10.1103/PhysRevB.81.115422 PACS number(s): 78.67.Ch, 68.65.−k

I. INTRODUCTION

The understanding of the phonon dispersion,[1–6] Kohn anomalies,[7–11] resonant Raman scattering,[12–17] and trigonal warping effects[18,19] in single-walled carbon nanotubes (SWNTs) has progressed significantly since the first report of resonant Raman scattering in SWNTs in 1997.[2] Symmetry-allowed, first-order scattering from the low-frequency radial breathing mode (RBM) and several higher-frequency tangential modes (the G band) is particularly strong when the photon energy resonates with important exciton or interband electronic transitions of a particular tube.[20] In resonance, individual SWNTs can be studied with less than ~1 mW of laser power.[13,20,21]

Here we report a systematic experimental study of the effect of bending curvature on the local Raman scattering spectrum of SWNTs. Previous theoretical studies have shown that bending changes the electronic properties of SWNTs.[22–26] Of particular significance for our experimental study here is recent theoretical work by Malola *et al.*[27] on Raman-active phonons in bent SWNTs, which shows how bending curvature in a SWNT shifts the Raman-mode frequencies and activates previously symmetry-forbidden modes. Recently, changes in the resistance of a SWNT associated with a bend or a loop have also been reported.[28–30] Preliminary reports of Raman scattering established the quality of SWNTs involved in these resistance studies.[28]

II. EXPERIMENTAL DETAILS

SWNTs were grown by chemical-vapor deposition at 900 °C using a mixture of CH_4 and H_2 (ratio 1:2) at 10–100 standard cubic centimeters per minute as the carbon feedstock and Fe/Mo adsorbed on alumina nanoparticles as the catalyst. Details of growth appear in a previous publication.[29] The alumina/Fe/Mo particles were supported on an ST-cut (i.e., miscut) single-crystal quartz substrate that was annealed at 900 °C for 8 h in air prior to nanotube growth to form atomic-scale step edges at the surface.

Scanning electron microscopy (FESEM LEO 1530) at low acceleration voltage (~1 kV) was used to map the serpentine path of the filament within the plane of the substrate, as shown in the left panel of Fig. 1. The term "filament" is used to describe a serpentine structure that may consist of an individual single-walled nanotube or a small bundle of a few parallel tubes. Atomic force microscope (AFM) (PSIA, XEI-100) topographic images such as that given in the right panel of Fig. 1 were collected to measure the height of a filament and hence estimate the number of tubes inside.

Raman spectra were collected at room temperature in air at various points along one filament using a single-grating microRaman spectrometer (Renishaw inVia microRaman system) equipped with a computer-controlled sample stage (~30 nm/step), tandem holographic edge filters, 100× objective and an air-cooled charge-coupled device. The quartz substrate with serpentine SWNTs was mounted on a rotary stage on top of the microscope stage. The focal spot diameter at the sample position was approximately 0.8 μm. Experiments were carried out using low laser power

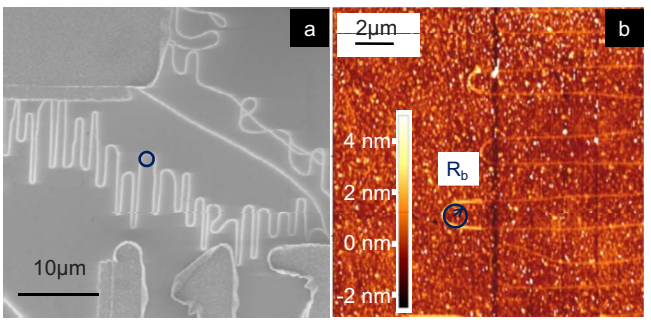

FIG. 1. (Color online) (a) SEM and (b) AFM images of serpentine nanotubes on quartz substrate. The circles indicate the bending radius R_b.

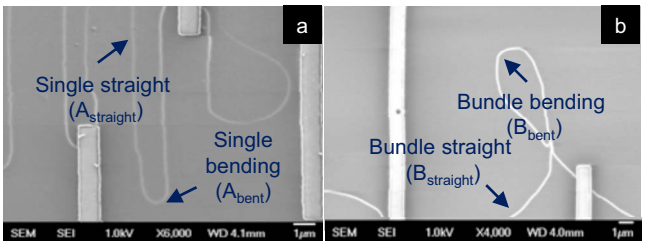

FIG. 2. (Color online) SEM images of (a) a single serpentine shaped SWNT and (b) a bundle of SWNTs forming a loop.

($P \sim 1$ mW/μm^2) with 647.1, 514.5, and 488.0 nm excitations. Specific positions on a filament were obtained by superimposing the SEM and Raman microprobe images, since the metal contacts can be seen in both. The highest backscattering intensity for the strongest SWNT Raman band near $\sim$1590 cm^{-1} (i.e., in the G band) was achieved when the incident polarization was approximately tangential to the filament axis at the center of the focal spot. The intensity of the G band was then optimized through a combination of small orthogonal translations of the microscope stage and rotations of the rotary stage after the approximate focal position was obtained. The incident laser was polarized parallel to the polarization component passed by the analyzer.

III. RESULTS AND DISCUSSION

When a SWNT is in resonance with the laser line, the local Raman spectrum from the focal spot can be followed from point to point along the filament, i.e., from the straight segments to the nearly circular bends. Raman spectra typical of high-quality tubes were observed: a narrow RBM in the frequency range from 100 to 300 cm^{-1}, a weak and broad D band between 1300 and 1400 cm^{-1} and a high-intensity G band with several components around 1585 cm^{-1}. The average radius of bending curvature was estimated by fitting a circle to each bend, as imaged by SEM or AFM, as in Fig. 1.

Significant changes in band frequency were observed along the length of a filament, correlated with the curvature of the bend. First we describe the detailed Raman spectra of two typical cases, later we present detailed trends in curvature dependence for a larger population of bent filaments. Local Raman spectra were collected from the positions labeled A_{bent}, $A_{straight}$, B_{bent}, $B_{straight}$ in the SEM images of Figs. 2(a) and 2(b). Figure 2(a) depicts what we presume is an individual SWNT while Fig. 2(b) is likely a small bundle of SWNTs. The assignment of Fig. 2(a) to an individual SWNT is based on the fact that the AFM height of this filament is 1.6 nm and only one RBM frequency is observed. It may be a small bundle containing 2 or 3 tubes of similar radius lying adjacent and parallel on the substrate but this would not affect our essential conclusions. The AFM height for Fig. 2(b) is 11 nm and two distinct RBM frequencies are observed. Hence this filament must be a small bundle of SWNTs, containing roughly 10–20 tubes.

Figure 3 displays the RBM, D, G, and 2D Raman bands from these straight and gently bent segments, with R_b=0.8 μm (for A) and 3 μm (for B). The low-frequency

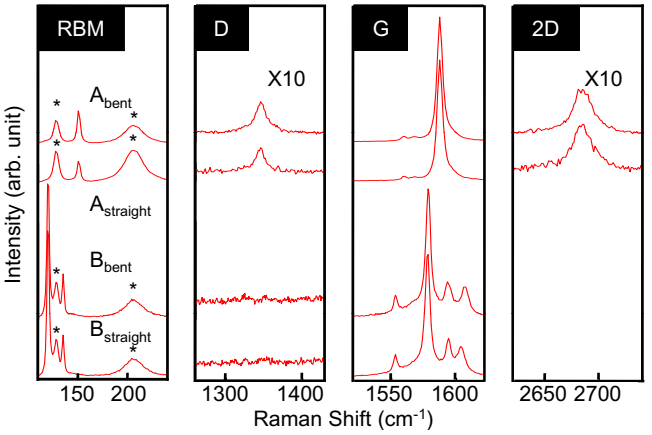

FIG. 3. (Color online) Raman spectra collected from a single tube (A_{bent} and $A_{straight}$) using laser line 514 nm and from a bundle (B_{bent} and $B_{straight}$) using laser line 647 nm. The respective positions A_{bent}, $A_{straight}$, B_{bent}, $B_{straight}$ are illustrated in Figs. 2(a) and 2(b). The starred features are from the substrate. Spectra in the D-band and 2D-band regions are magnified by a factor of 10.

radial breathing mode, broader defect-induced D band near 1350 cm^{-1}, bands derived from the doubly degenerate high-frequency G mode of graphite near 1582 cm^{-1}, and a two-phonon symmetry-allowed 2D band near 2700 cm^{-1} are all visible. We first discuss the overall character of the spectra from straight and bending segments, from which the metallic or semiconducting character and structural quality of the nanotubes can be deduced. The Raman spectra at A_{bent} and $A_{straight}$ from a putative single SWNT were excited by 514.5 nm radiation. The spectrum at $A_{straight}$ has just one RBM, at 151 cm^{-1}, with a full width at half maximum of $\sim$4 cm^{-1} (including instrumental broadening of $\sim$1 cm^{-1}). This frequency implies a tube diameter $d \sim 1.6$ nm using the relation ω_{RBM}=[204 cm^{-1} nm]/d+27 cm^{-1}.[16,31–33] The RBM mode at A_{bent} is upshifted slightly, by $\sim$2 cm^{-1}, compared to $A_{straight}$. Since the RBM frequency for SWNTs supported on or suspended above a SiO_2/Si substrate have the same dependence on d,[31] the observed upshift likely cannot be ascribed to the bent region losing contact with the substrate. The D band at both A_{bent} and $A_{straight}$ is very weak, only about 1/100th of the G-band intensity. The narrowness of the RBM and the weakness of the D band both imply that this SWNT is relatively defect-free. The narrow G^- components at both A_{bent} and $A_{straight}$ reveal this sample to be a semiconducting SWNT.[20,21] The feature at $\sim$2685 cm^{-1}, called the G′ band or 2D band, is not associated with defects, but is allowed even in well-ordered SWNTs due to two-phonon scattering. Since the 2D band has the highest frequency, the small shift of the peak frequency between straight and bent segments is the most apparent here.

The spectra collected from B_{bent} and $B_{straight}$ with 647 nm excitation arise from a small bundle of SWNTs. Two RBM modes at 120 and 136 cm^{-1} corresponding to $d \approx 2.2$ nm and $d \approx 1.9$ nm are observed with a full width at half maximum of $\sim$3 cm^{-1}. Very weak or no D-band scattering is observed from both locations. The G band shows more peaks than are seen from a single SWNT. Since the four strongest G-band components are all narrow, we can assume that the

bundle contains no metallic SWNTs in resonance with the laser. It is possible that either or both of the two highest-frequency G-band components are actually associated with a double-resonant D′ band, which involves an intravalley double-resonant process.[34,35] The next highest intensity component in the G band, at ~1575 cm^{-1}, can be assigned to the G^+ mode. Its frequency is considerably downshifted from what is normally observed, i.e., 1587–1592 cm^{-1}.[20,21,36,37] Also note that the G^+ mode excited by a 514 nm laser line at A_{bent} and $A_{straight}$ is also slightly downshifted. In contrast, a 488 nm laser produces an upshifted G^+ band at 1604 cm^{-1} for filaments on ST-quartz synthesized in the same manner (not shown here). Since the frequency of the G^+ mode is the lowest (~1575 cm^{-1}) when excited by the lowest-energy laser line (647 nm) and highest (~1604 cm^{-1}) when excited by the highest-energy laser line (488 nm), it is tempting to correlate this behavior with the dispersion relation of the Raman G mode, as reported by Maultzsch *et al.*[38] However, it must be noted that these shifts of frequency occur across different nanotubes. Resonant Raman scattering study on *one* single SWNT reported by Jiang *et al.*[37] failed to observe any shift of the G-band frequency with respect to different laser lines. Hence we propose that the observed frequency shift of G^+ mode with laser energy for different nanotubes comes from a difference in resonance condition: i.e., nanotubes that resonate with higher-energy lasers exhibit higher-frequency G bands.

A. Curvature dependence of Raman modes for gently bent nanotubes

At the frequency scale of Fig. 3 the difference between straight and bent segments of the same serpentine tube is difficult to see. Nevertheless, by fitting the spectra to Lorentzian components, small systematic changes in the RBM, D, G, and 2D (G′) bands are revealed for a series of samples. Figure 4 plots the results for two filaments (different from those in Fig. 3) as a function of the dimensionless bending factor $\Theta = d/2R_b$. Θ is the relative length difference between the inner and outer walls of a SWNT of diameter d as it circuits a bend of radius R_b. Here we study gently bent filaments with $0 < \Theta < 0.0025$, first focusing on two illustrative cases (one semiconducting, one metallic) and then presenting an overview of results for the full sample of seven serpentine filaments. Figure 4(a) shows the frequencies of the RBM, D, G, and 2D band components versus Θ obtained from what is likely an individual semiconducting SWNT (as determined by the single RBM peak and the sample's AFM height). The right side of Fig. 4 gives the frequencies of the RBM and the G-band components as a function of Θ for a bundle containing two metallic SWNTs. Although the metallic nanotubes exhibit a Breit-Wigner-Fano line shape in the G-band components, we still fit them with a Lorentzian line shape as an approximation. The linear least-squares fits (dashed lines) exclude the data with high scatter at the lowest curvatures. The data at higher curvature is well described by a function linear in Θ while the data for straight or weakly bent sections show a strong stochastic component of unknown origin. A resonant Raman study of SWNTs synthesized by a similar

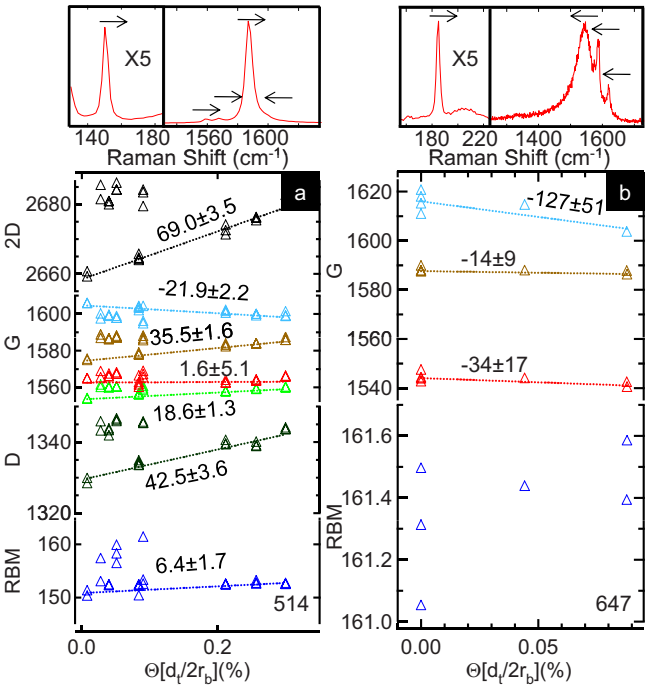

FIG. 4. (Color online) (a) Frequencies (cm^{-1}) of Raman RBM, D, G, and 2D bands as a function of Θ for a single semiconducting SWNT collected under 514 nm laser excitation. (b) Frequencies (cm^{-1}) of Raman RBM and G bands as a function of Θ for a metallic SWNT bundle collected under 647 nm laser excitation. The signal from the nanotube bundle is dominated by one metallic nanotube. The numbers next to the fitting lines indicate the slope of the lines. The upper left and right panels show the Raman spectra of the filaments studied in (a) and (b), respectively. The arrows in the spectra show the directions that the peaks move with increasing bending curvature.

method also shows small stochastic shifts in the peak position of ±5 cm^{-1} along the length of the nanotube.[37] We attribute this uncontrolled variation to unknown local defects that arise during synthesis. The smaller relative deviations from the linear fit in Fig. 4(a) as compared to (b) are due to larger amount of data collected from this filament.

Theoretically, the shift for the 2D band should be double of that for D band since $\omega_{2D} \approx 2\omega_D$. We obtain $d\omega_{2D}/d\Theta \sim 1.6 d\omega_D/d\Theta$, a discrepancy that we ascribe to the stochastic variations described above. The RBM mode shows the least shift in frequency with respect to curvature.

We have observed shifts of Raman frequencies linear in bending curvature for seven different serpentine SWNT filaments, including both individual SWNTs and SWNTs in bundles. Table I summarizes these results. The parameter $\alpha \equiv d(\ln \omega)/d\Theta$ provides a convenient dimensionless measure of the sensitivity to bending: the fractional shift in mode frequency for a given fractional nanotube shear due to bending. Across these seven filaments, α varies from −0.08 to +0.04. What is the source of this pronounced diversity in bending response? Malola *et al.*[27] used a combination of density-functional-based tight-binding and nonresonant bond polarization theory to calculate the Raman mode frequencies and intensities as a function of Θ from 0 to 0.04. Due to an overestimate of the bond stiffness, the calculated Raman fre-

TABLE I. Normalized shifting parameter $\alpha \equiv d(\ln \omega)/d\Theta$ for G band (only A modes), D, D′, and 2D band measured from seven SWNT filaments. The RBM frequencies (in cm^{-1}) and tube diameters (in nm) are also given. "s" means semiconducting and "m" means metallic.

Single nanotubes							
Type	RBM frequency	Tube diameter	α_{A1} [a]	α_{A2}	α_{A3}	α_{D}	α_{2D}
s	150	1.66	0.012	0.023	−0.014	0.032	0.026
s	157	1.57	0.001	−0.001	−0.020		

Nanotube bundles							
Type	RBM frequencies	Estimated Tube Diameter[b]	α_{A1}	α_{A2}	α_{A3}	α_{A4}	$\alpha_{D'}$
s	155, 167, 196	1.5	0.004	0.006			
s		1.3	−0.003	0.003	−0.003	0.004	
s		1.3	−0.008	0.002	0.002	0.011	
s		1.3	−0.014	−0.012	−0.013	−0.007	−0.069
m	185, 161	1.4	−0.021	−0.008			−0.073

[a] α_{A1} is the shifting parameter for the lowest-frequency A mode observed in the G-band region.
[b] This is the average tube diameter used to calculate α.

quencies are all ~13% too high, but the use of α obviates this discrepancy. For gentle bending, some of the Raman modes shift upward with bending, others downward; these curvature sensitivities also depend on tube wrapping indices (n,m). Since we cannot identify the specific (n,m) of our tubes, we consider the overall variance of the bending response for an ensemble of possible tubes. The theoretical results for the Raman G modes of (13,0), (6,6), and (13,4) nanotubes span a range $-0.04 < \alpha < 0.02$ while the theoretical frequency for the RBM is nearly independent of bending. Taking into account that our experimental results must sample more nanotubes of various (n,m) than were studied theoretically, the observed dispersion $-0.08 < \alpha < 0.04$ is reasonably consistent with theory. This conclusion is more convincing when one considers that the dependence of tube band gap on bending also depends strongly on nanotube wrapping indices in theory,[26] as does the strain-induced shift in Raman frequency in experiment.[13]

B. Symmetry breaking in sharply bent nanotubes

In one filament, the bending curvature is very strong: $R_b = 50$ nm and $\Theta \sim 0.013$. As a result of this strong bending curvature, the G-band fragments into a multitude of narrow peaks depicted in Fig. 5(a), many more than previously observed in any straight or gently bent nanotube. The data were collected in the same manner as described before with the incoming laser polarized along the local tube axis. The straight segment of the same filament has an unremarkable G-band spectrum, with a consistent shape at several locations along the filament; Fig. 5(b) provides a typical example. This filament exhibits three RBM modes at 109, 151, and 190 cm^{-1} with $d \sim 2.5$ nm, 1.6 nm, and 1.3 nm, respectively, as shown in the inset of Fig. 5(b). Hence this filament contains at least three distinct nanotubes. We fit the spectrum to 14 Lorentzian peaks, drawn as dotted lines in Fig. 5(a). This unique G-band line shape apparently arises from the broken cylindrical symmetry caused by the sharp bend. Theory predicts that symmetry-forbidden modes such as E_1, E_2 and E_3 emerge as the bend curvature breaks the azimuthal symmetry in the nanotube.[27] The complex line shape of Fig. 5(a) is a superposition of such contributions from at least three nanotubes. The width of the entire complex, from 1510 to 1670 cm^{-1}, is 0.063 times the frequency of the strongest G-band peak in the straight segment (i.e., the fractional

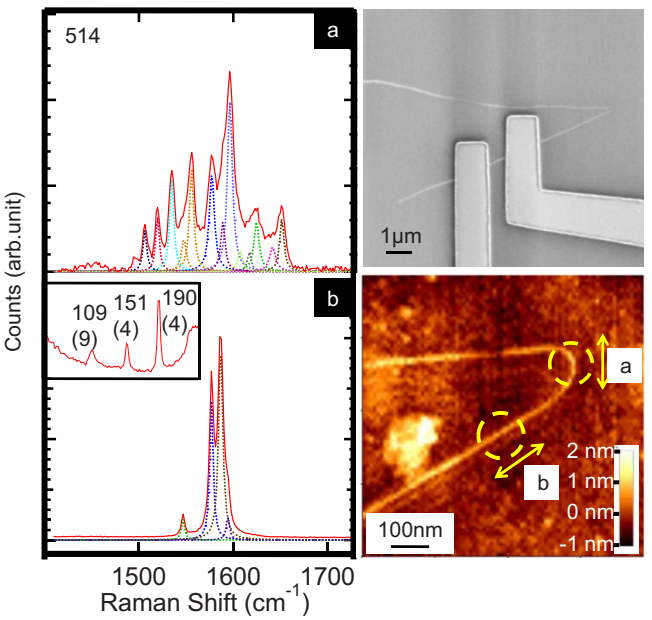

FIG. 5. (Color online) Left panel: Raman spectra collected from a nanotube bundle (a) at a sharp kink and (b) along its straight segment. The inset shows three RBM peaks observed on this small bundle. Right top: SEM image of the kink. Right bottom: AFM image with dashed circles showing laser positions and arrows showing polarization directions. The SWNT filament is on a Si/SiO_2 substrate with Pd electrodes attached.

width is 0.063). In the calculation of Malola *et al.* the fractional width of the symmetry-broken G-band complex at the experimental bending coefficient of $\Theta=0.013$ depends on the wrapping indices of the tube in question, varying from approximately 0.027 for (13, 0) and (6, 6) nanotubes to 0.04 for the (13, 4) nanotube. Hence the width of our experimental spectrum, which superposes contributions from at least three tubes, is consistent with the computed values.

IV. CONCLUSION

In conclusion, we have demonstrated a correlation between frequency shifts in the RBM, D, G, and 2D band and the nanotube bending factor $\Theta=d/2R_b$. From our experimental results we calculated the dimensionless shifting parameter $\alpha\equiv d(\ln\omega)/d\Theta$ for the Raman modes of seven SWNT filaments. The parameter α ranges from −0.08 to +0.04 for all the Raman modes studied, while that from theoretical calculation for three nanotubes ranges from −0.04 to +0.02. Considering that the bending sensitivities for Raman modes depends on nanotube wrapping indices (n,m), our results are reasonably consistent with the calculation. One particularly sharp bend ($\Theta\approx0.013$) on a small bundle of semiconducting nanotubes strongly breaks the nanotubes' azimuthal symmetry and hence activates several new G-band lines which are symmetry forbidden in the pristine straight nanotubes, as predicted by the theory. The resultant "broadening" of the G band shows a normalized width of 0.063. This result, as a superposition of contributions from at least three tubes, is also reasonably consistent with theoretical expectations. It provides a direct experimental observation of Raman activation through the breaking of cylindrical symmetry in nanotubes.

ACKNOWLEDGMENTS

This work was supported in part by NSF NIRT ECS 06-09243. We thank G. Mahan for reading and revising the paper. SEM images were taken in the Nanofabrication Laboratory of Penn State University.

*Corresponding author: www.phys.psu.edu/people/crespi.html

[1] R. A. Jishi, L. Venkataraman, M. S. Dresselhaus, and G. Dresselhaus, Chem. Phys. Lett. **209**, 77 (1993).
[2] A. M. Rao, E. Richter, S. Bandow, B. Chase, P. C. Eklund, K. A. Williams, S. Fang, K. R. Subbaswamy, M. Menon, A. Thess, R. E. Smalley, G. Dresselhaus, and M. S. Dresselhaus, Science **275**, 187 (1997).
[3] R. Saito, T. Takeya, T. Kimura, G. Dresselhaus, and M. S. Dresselhaus, Phys. Rev. B **57**, 4145 (1998).
[4] M. S. Dresselhaus and P. C. Eklund, Adv. Phys. **49**, 705 (2000).
[5] R. Saito, A. Jorio, J. H. Hafner, C. M. Lieber, M. Hunter, T. McClure, G. Dresselhaus, and M. S. Dresselhaus, Phys. Rev. B **64**, 085312 (2001).
[6] G. D. Mahan and G. S. Jeon, Phys. Rev. B **70**, 075405 (2004).
[7] S. Piscanec, M. Lazzeri, F. Mauri, A. C. Ferrari, and J. Robertson, Phys. Rev. Lett. **93**, 185503 (2004).
[8] S. Piscanec, A. C. Ferrari, A. Lazzeri, F. Mauri, and J. Robertson, AIP Conf. Proc. **786**, 424 (2005).
[9] R. Barnett, E. Demler, and E. Kaxiras, Phys. Rev. B **71**, 035429 (2005).
[10] P. M. Rafailov, J. Maultzsch, C. Thomsen, and H. Kataura, Phys. Rev. B **72**, 045411 (2005).
[11] H. Farhat, H. Son, G. G. Samsonidze, S. Reich, M. S. Dresselhaus, and J. Kong, Phys. Rev. Lett. **99**, 145506 (2007).
[12] M. S. Dresselhaus, A. Jorio, A. G. Souza Filho, G. Dresselhaus, and R. Saito, Physica B **323**, 15 (2002).
[13] S. B. Cronin, A. K. Swan, M. S. Unlu, B. B. Goldberg, M. S. Dresselhaus, and M. Tinkham, Phys. Rev. B **72**, 035425 (2005).
[14] R. Saito, A. Jorio, A. G. Souza Filho, G. Dresselhaus, M. S. Dresselhaus, A. Grüneis, L. G. Cançado, and M. A. Pimenta, Jpn. J. Appl. Phys., Part 1 **41**, 4878 (2002).
[15] C. Thomsen and S. Reich, *Light Scattering in Solids Ix* (Springer-Verlag, Berlin, 2007), Vol. 108, p. 115.
[16] A. Jorio, M. A. Pimenta, A. G. Souza Filho, R. Saito, G. Dresselhaus, and M. S. Dresselhaus, New J. Phys. **5**, 139 (2003).
[17] S. M. Bachilo, M. S. Strano, C. Kittrell, R. H. Hauge, R. E. Smalley, and R. B. Weisman, Science **298**, 2361 (2002).
[18] S. Reich and C. Thomsen, Phys. Rev. B **62**, 4273 (2000).
[19] R. Saito, G. Dresselhaus, and M. S. Dresselhaus, Phys. Rev. B **61**, 2981 (2000).
[20] M. S. Dresselhaus, G. Dresselhaus, A. Jorio, A. G. Souza Filho, and R. Saito, Carbon **40**, 2043 (2002).
[21] A. Jorio, A. G. Souza Filho, G. Dresselhaus, M. S. Dresselhaus, A. K. Swan, M. S. Ünlü, B. B. Goldberg, M. A. Pimenta, J. H. Hafner, C. M. Lieber, and R. Saito, Phys. Rev. B **65**, 155412 (2002).
[22] A. Rochefort, P. Avouris, F. Lesage, and D. R. Salahub, Phys. Rev. B **60**, 13824 (1999).
[23] M. Buongiorno Nardelli and J. Bernholc, Phys. Rev. B **60**, R16338 (1999).
[24] A. Maiti, A. Svizhenko, and M. P. Anantram, Phys. Rev. Lett. **88**, 126805 (2002).
[25] A. A. Farajian, H. Mizuseki, and Y. Kawazoe, Physica E **22**, 675 (2004).
[26] L. F. Chibotaru, S. A. Bovin, and A. Ceulemans, Phys. Rev. B **66**, 161401(R) (2002).
[27] S. Malola, H. Hakkinen, and P. Koskinen, Phys. Rev. B **78**, 153409 (2008).
[28] N. Geblinger, A. Ismach, and E. Joselevich, Nat. Nanotechnol. **3**, 195 (2008).
[29] J. Huang and W. Choi, Nanotechnology **19**, 505601 (2008).
[30] F. Léonard, F. E. Jones, A. A. Talin , and P. M. Dentinger, Appl. Phys. Lett. **86**, 093112 (2005).
[31] J. C. Meyer, M. Paillet, T. Michel, A. Moréac, A. Neumann, G. S. Duesberg, S. Roth, and J.-L. Sauvajol, Phys. Rev. Lett. **95**, 217401 (2005).
[32] M. Paillet, T. Michel, J. C. Meyer, V. N. Popov, L. Henrard, S. Roth, and J.-L. Sauvajol, Phys. Rev. Lett. **96**, 257401 (2006).
[33] M. S. Dresselhaus, G. Dresselhaus, R. Saito, and A. Jorio, Phys. Rep. **409**, 47 (2005).

[34] M. A. Pimenta, G. Dresselhaus, M. S. Dresselhaus, L. G. Cançado, A. Jorio, and R. Saito, Phys. Chem. Chem. Phys. **9**, 1276 (2007).
[35] R. Saito, A. Jorio, A. G. Souza Filho, G. Dresselhaus, M. S. Dresselhaus, and M. A. Pimenta, Phys. Rev. Lett. **88**, 027401 (2001).
[36] A. M. Rao, S. Bandow, E. Richter, and P. C. Eklund, Thin Solid Films **331**, 141 (1998).
[37] C. Y. Jiang, J. L. Zhao, H. A. Therese, M. Friedrich, and A. Mews, J. Phys. Chem. B **107**, 8742 (2003).
[38] J. Maultzsch, S. Reich, U. Schlecht, and C. Thomsen, Phys. Rev. Lett. **91**, 087402 (2003).